
Article:
Gardy, J, Hassanpour, A, Lai, X et al. (2017) Biodiesel production from used cooking oil using a novel surface functionalised TiO2 nano-catalyst. Applied Catalysis B: Environmental, 207. pp. 297-310. ISSN: 0926-3373

https://doi.org/10.1016/j.apcatb.2017.01.080

Title: Biodiesel production from used cooking oil using a novel surface functionalised TiO_2 nano-catalyst

Author: Jabbar Gardy Ali Hassanpour Xiaojun Lai Mukhtar H. Ahmed Mohammad Rehan

PII: S0926-3373(17)30097-8
DOI: http://dx.doi.org/doi:10.1016/j.apcatb.2017.01.080
Reference: APCATB 15393

To appear in: *Applied Catalysis B: Environmental*

Received date: 29-11-2016
Revised date: 11-1-2017
Accepted date: 28-1-2017

Please cite this article as: J. Gardy, A. Hassanpour, X. Lai, M.H. Ahmed, M. Rehan, Biodiesel production from used cooking oil using a novel surface functionalised TiO_2 nano-catalyst, *Applied Catalysis B, Environmental* (2017), http://dx.doi.org/10.1016/j.apcatb.2017.01.080

Biodiesel production from used cooking oil using a novel surface functionalised TiO_2 nano-catalyst

Jabbar Gardy[1], Ali Hassanpour[1, †], Xiaojun Lai[1], Mukhtar H. Ahmed[2], Mohammad Rehan[1, 3]

[1]School of Chemical and Process Engineering, University of Leeds, LS2 9JT Leeds, UK.

[2]Nanotechnology Integrated Bioengineering Centre, University of Ulster, Jordanstown, BT37 0QB Belfast, UK.

[3]Centre of Excellence in Environmental Studies (CEES), King Abdulaziz University, Jeddah, Saudi Arabia.

[†] Corresponding author: Tel.: +441133432405; E-mail: a.hassanpour@leeds.ac.uk

Highlights

- A novel, efficient and recyclable mesoporous $TiO_2/PrSO_3H$ solid acid nano-catalyst was synthesised.
- We examined the catalytic activity, stability and reusability of synthesised mesoporous $TiO_2/PrSO_3H$.
- The FAME yield from UCO was 98.3% under optimum process conditions.
- Synthesised biodiesel from UCO satisfied ASTM D6751 and EN 14214 standards.

ABSTRACT

A novel, efficient and recyclable mesoporous $TiO_2/PrSO_3H$ solid acid nano-catalyst was synthesised by the post-synthetic grafting of propyl sulfonic acid groups onto a mixed phase of a TiO_2 support. The synthesised nano-catalyst was characterised using FTIR, SEM, TEM, XPS, N_2 adsorption–desorption isotherms, XRD, DSC, TGA, and CHNS analysis. The percentage of loading for propyl sulfonic acid on the TiO_2 support was calculated using CHNS analysis and TGA. The catalytic performance of $TiO_2/PrSO_3H$ on the production of the fatty acid methyl esters (FAME) via simultaneous esterification and transesterification reactions from used cooking oil (UCO) has been studied. The effects of different process parameters showed that 98.3% of FAME can be obtained after 9 hrs of reaction time with 1:15 molar ratio of oil to methanol, 60°C reaction temperature and 4.5 wt% catalyst loading. It was also found that the one-pot post-surface functionalisation strategy with hydrophilic functional groups ($-SO_3H$) enhanced the acid strengths of the nano-catalyst providing more acid sites for the reactants, and improving the accessibility of methanol to the

triglycerides (TG)/free fatty acids (FFAs) by increasing the pore volumes/sizes of the nano-catalyst. The solid acid nano-catalyst was re-used in four consecutive runs without significant loss of catalytic efficiency. Finally, the synthesised biodiesel fuel satisfied ASTM and EN standards.

KEY WORDS

TiO_2/propyl sulfonic acid; solid acid nano-catalyst; esterification & transesterification; biodiesel; used cooking oil

1. INTRODUCTION

Nanomaterials have fascinating and unique properties for the usage in various industrial fields. Titanium dioxide nanoparticles (TiO_2 NPs) are among the most widely studied for their use in photocatalysis, gas sensors, medicine, catalyst support, pigments, cosmetics and solar cells [1-3]. This is due mainly to their favourable properties, acidity, wide band gap, high surface area, low cost and highly availability, better redox selectivity, good mechanical and chemical stability, high reactivity, low toxicity, and high reusability [4-6]. TiO_2-NPs naturally occur in three main crystallographic phases, these being anatase, rutile, and brookite [2], but the most commonly used, because of its highly photocatalytic activity properties, is a mixture of anatase and rutile phases of TiO_2 [7].

Because of their multiple potential applications, straightforward recoverability and excellent properties, a wide range of recent studies on synthetic routes have been undertaken to fabricate surface modified nanoparticles in order to increase their surface acidity/basicity [8-13]. This is of particular significance in relation to nano-catalysts for biodiesel production involving the use of cheap raw materials containing free fatty acids (FFAs) as the acid catalysts can facilitate simultaneous esterification of FFAs and transesterification of triglycerides without soap formation [14, 15]. In the context of green chemistry, recycled vegetable oils could be used as inexpensive feedstocks for biodiesel fuel production [16-18]. Such use helps to reduce environmental pollution and utilises economies for cheap biodiesel production [19-21]. The yield and quality of biodiesel can be highly affected by the surface area, surface acidity/basicity, and particle size of the catalysts used in the esterification and/or transesterification processes [22]. This has encouraged the development of novel recyclable solid acid nano-catalysts to replace conventional corrosive homogeneous acid catalysts [21, 23], which can corrode reactors and requires further washing with neutralisation steps for their removal from the biodiesel and its by-products [24].

According to the literature, the surface modification of nanoparticles could create solid acid nano-catalysts [25]. The surface modification could be carried out through different strategies such as chemical treatments, ozonolysis, polymer grafting, encapsulation in a silica shell (silanization), ligand exchange technique, or capping agents (surfactants)/encapsulation in a surfactant corona [26, 27]. Modification of the surface of nanoparticles by integration of acidic functional groups (e.g. $-SO_3H$) to produce solid acid catalysts for different applications has been highlighted in the literature over the recent years [8, 11, 21, 24, 28-38]. This is because sulfonic acid functional groups on the surface of nanoparticles lead to the formation of porous materials with high accessibility to the active sites [39].

There are several recent works describing the performance of such promising materials for the biodiesel production [10, 19, 31, 40-42]. The surface modification of mesoporous materials, such as SBA-15, with organosilane sulfonic groups increases the hydrophobic character of the solid acid catalyst surface resulting in high catalytic activity and selectivity toward glycerol in the esterification of FFAs [43]. However, these types of catalysts are quite sensitive to the presence of impurities in raw materials such as recycled oil feedstocks [44]; also, low sulfonic acid sites loading on the surface of nanoparticles are hampered in practical application of such catalysts [37]. Furthermore, fast deactivation is another practical problem for such catalyst. Therefore, there is a need to synthetize stronger and more tolerant nano-catalysts with higher re-usability for cheap feedstocks such as used cooking oil.

There are, so far, no reports on the surface functionalisation of titania with 1,3-propyl sultone for a direct-preparation of propyl-sulfonic acid grafting the surface of TiO_2 NPs and/or on the use of such material as a solid acid nano-catalyst for biodiesel production. Therefore, the present work describes the fabrication, characterisation and application of a novel TiO_2-propylsulfonic acid nano-catalyst in order to understand the impact of catalytic activity and reusability of such nano-catalyst on biodiesel production from used cooking oil (UCO) as a

cheap feedstock. Finally, the synthesised biodiesel from the catalytic esterification/transesterification processes was analysed in accordance to ASTM and EN standard methods.

2. EXPERIMENTAL

2.1 Materials and methods

2.1.1 Synthesis of solid acid nano-catalysts

The surface charge of titania NPs is pH dependent. Therefore, we pre-treated the titania NPs with aqueous solution of ammonium hydroxide to reduce the agglomeration and increase the receptor sites ($TiO_2 + nOH^- \longrightarrow TiO_2(OH)n^{n-}$) on the surface of titania support [45]. 6g of TiO_2 NPs (Sigma-Aldrich) was added slowly into a 50ml of 0.5M ammonium hydroxide solution (Sigma-Aldrich) at room temperature. The suspension was then sonicated for 30mins. The resultant was transferred into a centrifuge tube for washing with double deionised water and dried at 80°C for 4 hrs in an oven. Typically, 1g of the dried powder was charged into a three necked glass flask at ambient temperature then 20ml suspension solutions of 0.1 molar 1,3-propane sulfone (Sigma-Aldrich) in dry toluene (Sigma-Aldrich) was added dropwise. The resultant suspension was slowly stirred under reflux for 72 hrs at 120°C. The synthesized TiO_2-propyl sulfonic acid powders were cooled to room temperature. Thereafter the synthesised nano-catalyst was separated from the solution using a centrifuge and washed off several times with fresh toluene to remove the remained unreacted 1,3-propane sulfone. The resulting precipitate sample was dried overnight at 80°C then denoted sample as $TiO_2/PrSO_3H$.

2.1.2 Synthesis of biodiesel fuel

The simultaneous esterification and transesterification of UCO was performed in a glass batch reactor connected with an automatic temperature controller loop system under constant agitation rate at 600 RPM using a digital mechanical stirrer and a reflux condenser. The sample of UCO obtained from a local restaurant in Leeds, UK, was pre-

treated by filtration process to remove solid impurities and heated to 100°C for a few hours to remove the moistures. Specified amounts of pre-treated UCO, $TiO_2/PrSO_3H$ nano-catalyst and methanol (Sigma-Aldrich) were charged into the batch reactor. The three-phase (solid-liquid-liquid) mixture was mixed at 600 RPM and heated to specified temperatures and times. The final reaction mixture was transferred into a separating funnel and allowed to cool to room temperature. A few millilitres of aliquot was withdrawn from the upper layer, biodiesel phase, and separated from the remaining impurities using a centrifuge at 9000 RPM for 10 mins to quantify the fatty acid methyl ester (FAME) content of the samples by off-line gas chromatography (GC) [4].

2.2 Characterization methods

2.2.1 Catalyst characterization

Physicochemical properties of the prepared $TiO_2/PrSO_3H$ and TiO_2 nano-catalysts were fully characterised as follows: Fourier transform infrared (FT-IR) spectroscopy was measured at room temperature using a Nicolet iS10 FT-IR spectrometer fitted with a DTGS-KBr detector. A minimum of 36 scans were performed at the average signal of infrared with a resolution 4 cm^{-1} in the ranges of 500 cm^{-1} to 4000 cm^{-1}. Particle size and surface morphologies were observed with a high performance cold field emission scanning electron microscopy (CFE-SEM, SU8230 Hitachi) and transmission electron microscopy (TEM, FEI Titan Themis Cubed 300). The location of the elements and elemental compositions of the prepared nano-catalyst sample were identified using the TEM fitted with high-angle annular dark field (HAADF) detector operated at an accelerating voltage of 300kV equipped with an energy dispersive X-ray spectroscopy (EDS, Oxford INCA 350). Nitrogen porosimetry was obtained at -196°C on a Micromeritics TriStar 3000 surface analyser. Prior to the measurements, the nano-catalyst sample was degassed in a vacuum oven overnight at 120°C. The X-ray

photoelectron spectroscopy (XPS) was performed using a KRATOS XSAM 800 equipped with an energy analyser and monochromated Al-Kα X-ray source (hv1486 eV) generated from aluminium anode. The film of the nano-catalyst sample was prepared by dissolving a few milligrams of catalyst sample in chloroform and methanol (3:1) then coating on the silicon wafer surface. CasaXPS version 2.3.17 was used for spectral fitting and binding energies corrected to the C 1s peak at 285 eV to compensate for residual charging effects. The bulk and surface sulfonic acid loadings on the surface of the nano-catalysts were determined via elemental analysis (Thermo Scientific™ FLASH 2000 CHNS Analyzer) and XPS, respectively. The thermal stability was carried out on a Mettler Toledo (TGA/DSC-1) star^{e} system. The system was programmed to heat up from 25°C to 900°C at 10°C/min under nitrogen gas at 50 ml/min with a constant flow rate. Total propyl sulfonic acid loadings were calculated from the TGA weight loss between 200^{o}C and 600^{o}C. XRD patterns were recorded on a Bruker D8 X-ray diffraction, fitted with a CuKα radiation (1.54Å, 40kV, 40mA). Data was collected from 2θ angle ranging of 10° to 70° with step size 0.0495° at 35 seconds per step.

2.2.2 Biodiesel characterization

The flash point of prepared biodiesel sample was measured by an auto ramp closed cup flash point tester (Setaflash series 3, England) equipped with a coolant block unit. The temperature ramped at 1°C-2°C/min until the flash was captured. Moreover, the pycnometeric method was used to determine the density of obtained biodiesel at 15°C. Furthermore, viscosity of prepared biodiesel was measured on a Bohlin-Gemini 150 rotary rheometer (Malvern, UK). Additionally, trace moisture content in biodiesel was analysed by volumetric Karl Fischer titration (Mettler Toledo-V20, Germany). The acid values and percentage of FFA were measured according to the standard methods [4]. The cloud point of prepared biodiesel was

examined by a differential scanning calorimetry (DSC 1, Mettler Toledo, UK) equipped with an intracooler system (Huber TC45). (5±2.5) mg of biodiesel sample was accurately weighted in a 40µl sealed standard aluminium pan and placed in the DSC sample chamber. The experiment was initiated by keeping the sealed sample pan at 50°C for 5 mins to homogenise the sample should it contain any wax materials. The system was then cooled to -30°C at 1°C/min and held at that temperature for 5 mins. The sealed sample pan was then heated to 50°C at 1°C/min and held at that temperature for 5 mins. Nitrogen gas, at a constant flow rate of 50ml/min, was used as a purge gas during all steps in this experiment and analysed using Mettler Star^{e} software. The cloud point was the onset temperature of the initial exothermic peak on the cooling curve. Finally, the thermal stability of prepared biodiesel was assessed on the Stanton Redcroft thermogravimetric analysis (TGA-TGH 1000) on 20-25 mg of biodiesel sample at 10°C/min during heating from 25°C to 700°C under air gas at 50ml/min with a constant flow rate.

3. RESULTS AND DISCUSSION

3.1 Catalyst characterisation

$TiO_2/PrSO_3H$ nano-catalyst was prepared by the reaction of TiO_2-NPs support with an extremely reactive sulfoalkylating agent to increase the surface acidity of TiO_2-NPs. The concentration of propyl sulfonic acid groups attached on the surface of TiO_2-NPs mainly depends on the amount of available –O-H terminated adsorption sites. Such surface modification was formed through a ring opening reaction of 1,3-propane sultone with nucleophile cleaving the carbon-oxygen bond as shown in proposed scheme 1.

Figure 1 illustrates the FT-IR spectra over the range 500–4000 cm^{-1}, corresponding to the TiO_2 (in red) and $TiO_2/PrSO_3H$ (in black) nano-catalysts. The FT-IR spectrum for $TiO_2/PrSO_3H$ nano-catalyst shows several extra peaks compared to TiO_2-NPs

spectrum. The broad band in the range of 500-626.4 cm^{-1} assigned to Ti-O stretching vibrations can be clearly observed in both spectra [46]. The appearance of a new strong peak at 1031 cm^{-1} assigned to the stretching vibration of S-O bond, whereas the band occurring at 1130 cm^{-1} corresponded to C-O stretching vibration [47]. Moreover, the existed band at 1198 cm^{-1} attributed to the C-C stretching vibration. The new extra two peaks appeared on the black spectrum at around 1275 cm^{-1} and 1362.5 cm^{-1} are considered to be a fingerprint of the S=O symmetric and asymmetric stretching vibrations, respectively, for sulfonic acid groups attachment on the surface of TiO_2-NPs [47]. Similarly, the new peaks located at 1416 cm^{-1} and 1447 cm^{-1} are attributed to the methylene groups [$–CH_2–$] bending in $PrSO_3H$ functional groups [47]. The region below 3000 cm^{-1} clearly showed two distinct peaks at 2886 cm^{1} and 2946 cm^{1} that are likely to represent the C-H stretching vibrations, representing symmetric and asymmetric modes respectively, for the $–CH_2–$ groups in $PrSO_3H$ functional groups [47, 48].

Furthermore, the weak absorption bands at 1640 cm^{-1} in TiO_2-NPs and 1712 cm^{-1} in $TiO_2/PrSO_3H$ belong to H-O-H symmetric vibration of the physisorbed water molecules on the surface. Whilst the region between 1975 cm^{-1} and 2160 cm^{-1} clearly showed few peaks related to the asymmetric stretching of CO_2 molecules adsorbed on the surface of the both $TiO_2/PrSO_3H$ and TiO_2 nano-catalysts [4, 49]. Additionally, the broad band at 3200-3500 cm^{-1} in $TiO_2/PrSO_3H$ nano-catalyst assigned to O-H stretching vibration of sulfonic acid functional groups on the surface of TiO_2-NPs [47].

Surface morphological and structure features of the TiO_2-NPs and $TiO_2/PrSO_3H$ nano-catalysts were examined by using Hitachi CFE-SEM. It is clear from Figure 2a that TiO_2-NPs have relatively uniform sized particles with some agglomerates. Moreover, the TiO_2-NPs exhibit mainly spherical like morphology distribution. $TiO_2/PrSO_3H$

nano-catalyst (see Fig. 2b), however, showed non-uniform particle size distributions with well-defined hexagonal, tetragonal and cubic shaped structures (inset SEM image @ 250K magnification). This may suggest that the surface modification caused slight enlargement of the particle sizes of TiO_2 support as can be seen clearly in Figure 2b (inset).

The particle size enlargements and different morphologies for $TiO_2/PrSO_3H$ nano-catalyst are also clearly seen in TEM images (Figure 3). $TiO_2/PrSO_3H$ agglomerated resulting in larger clusters owing to interaction between the head groups of $PrSO_3H$ on the surface of TiO_2-NPs. It is also important to mention that the enlarged particle sizes (red arrow) of as-synthesised $TiO_2/PrSO_3H$, observed in different TEM images, were due to the effects of surface grafting. The TEM images also show mixture of tetragonal/cubic/hexagonal morphologies of $TiO_2/PrSO_3H$ nano-catalyst with good crystallinity. The uniform and narrow particle size distributions of prepared nano-catalyst mainly depend on the initial TiO_2-NPs support with the grafting of 1,3-propane sultone into the surface of TiO_2 around the particle. A similar case has been reported for surface modification of different particles using silanization method [50]. The number based particle size distributions of $TiO_2/PrSO_3H$ were estimated from different TEM images and presented as histograms in Figure 4. These particles were found to have size range of 8.2-42 nm with an average particle size of 23.1 nm; whereas, the average particle size of initial TiO_2-NP was 22.34 nm [4].

HRTEM and SAED were conducted to investigate the particle morphologies as depicted in Figure 5a and b. As shown from the HRTEM images (Figure 5a), two different kinds of lattice fringes were observed, which were attributed to [101] interplanar spacing of anatase phase and [200] interplanar spacing of rutile phase with a tiny amorphous layer surrounding the surface of each particle. This indicates that [101]

and [200] facets have more preferable planes in anatase and rutile crystal phases, respectively. Noticeably, the *d*-spacing of the surface grafting nano-catalyst has expanded (inset in Figure 5a) with good core crystallinity regardless of the presence of $PrSO_3H$ groups on the surface. Furthermore, several obtained SAED patterns confirm the mixed phases of rutile and anatase with poly-crystallinities, in the $TiO_2/PrSO_3H$ nano-catalyst as shown in Figure 5b. In addition, the clear poly-crystallinity rings/spots correspond to the [101], [116], [004], [200], [220], [213], [216] and [204] lattice planes of anatase TiO_2 crystal phase in $TiO_2/PrSO_3H$ nano-catalyst. The other poly-crystallinity rings/spots, on the other hand, attributed to the [101], [210], [220], [310], [110], [200], [111], [202], [410], [221] and [202] lattice spacing of rutile TiO_2 crystal phase in $TiO_2/PrSO_3H$ nano-catalyst.

STEM electron energy loss spectroscopy (EELs)-maps for $TiO_2/PrSO_3H$ nano-catalyst was performed to obtain more information about the loading of carbon and sulphur layers on the surface of TiO_2-NPs. Titanium, carbon and sulphur maps were extracted from the spectrum imaging high loss region. Figure 6 demonstrates the high resolution elemental mapping of titanium, carbon and oxygen layer-by-layer distributions onto the $TiO_2/PrSO_3H$ particles. It can be observed that the surfaces of TiO_2-NPs are uniformly covered by carbon and sulphur layers. These homogenous distributions of carbon and sulphur clearly confirms the surface of TiO_2-NPs have been functionalised by $PrSO_3H$ groups. This also explains the reason for surface area reduction (Figure 7b) and some surface roughness of particles (Figure 5a). The STEM image further shows clear porous structures between $TiO_2/PrSO_3H$ particles.

Nitrogen adsorption–desorption isotherms and pore volume/size distributions of TiO_2 and $TiO_2/PrSO_3H$ samples are presented in Figure 7. The surface area was calculated from the nitrogen adsorption isotherms using the Brunauer–Emmett–Teller (BET)

method, but the mean pore size and total pore volume were calculated from the desorption branch of the isotherm using the Barrett-Joyner-Halenda (BJH) methods. The adsorption isotherms for both catalysts were determined in the range P/P_o=0.06-0.2, wherein a liner relationship was maintained, which revealed that both materials are typical type IV isotherms within mesoporous structure. The differences in condensation and evaporation were attributed to the monolayer-multilayer adsorption according to the IUPAC - behaviour, associated with mesoporous materials. The hysteresis loop shape for as-synthesised $TiO_2/PrSO_3H$ at relative pressure in the range of 0.75-0.985 was classified as H1-type, indicating a capillary condensation in mesoporous structure [51]. It should be noted from Figure 7 (inset) that the pore volume distributions in $TiO_2/PrSO_3H$ nano-catalyst has much larger mesopores with an increase of pore diameter compared with the initial TiO_2-NPs. The large pore size is much more preferable for minimizing diffusion limitations for long alkyl chain hydrocarbons in FFA/triglyceride (TG) in esterification and transesterification reactions [4, 14, 52].

The detailed analyses for texture properties using N_2 adsorption-desorption isotherms, percentage of carbon and sulphur contents using CHNS analysis, as well as the percentage of sulphur using TEM-EDS for prepared $TiO_2/PrSO_3H$ nano-catalyst, are summarized in Table 1. It was found that the loading of 1.41% of carbon and 0.28% of sulphur from $PrSO_3H$ groups on the surface of TiO_2-NPs was accompanied by a small decrease of the BET surface area with an increase of the pore volumes and sizes.

The surface chemistry of the TiO_2 and $TiO_2/PrSO_3H$ nano-catalysts was investigated by X-ray photoelectron spectroscopy (XPS) as shown in Figure 8. The XPS analysis provides valuable insight into the surface compositions and bonding environments for both nano-catalysts. The detailed high resolution XPS of the O 1s, S 2p, C 1s, and Ti 2p peaks for $TiO_2/PrSO_3H$ are presented in Figure 9. The O 1s core level spectrum

(Figure 9a) was de-convoluted into three Gaussian peaks centred at 530.4 eV, 31.75 eV and 533 eV indicating the presence of Ti=O, S=O and S-O/C-O, respectively. However, it was very difficult to distinguish between the contribution of the binding energy (BE) of the O 1s core-level for O-C and O-S bonds because both of species fell in the same energy regions [53]. The S 2p spectra (Figure 9b) were fitted with three Gaussian peaks centred at 164.4 eV, 166.3 eV and 167.4 eV assigned to the S-C, S=O and S-O, respectively, supporting the presence of $PrSO_3H$ groups on the surface [53]. Moreover, the high resolution C 1s XPS spectra (Figure 9c) included two Gaussian peaks centred at 285.1 eV and 286.4 eV which can reasonably be assigned to the C-C and C-S/C-O, respectively, in the $PrSO_3H$ groups [54]. The above findings indicate the surface of TiO_2-NPs is functionalised with $PrSO_3H$ groups. Figure 9d depicts the Ti $2p_{1/2}$-Ti $2p_{3/2}$ spin-orbit splitting at 464.4 eV and 458.7 eV, respectively, with a BE= 5.74 eV confirming the oxidation state of Ti in the as-prepared $TiO_2/PrSO_3H$ is IV [55-57]. The surface atomic ratios of Ti:O and S:C were determined from the XPS data and found to be 1:6.64 and 1:4.63, respectively. In fact, these ratios theoretically supposed to be 1:6 and 1:3 for Ti:O and S:C, respectively. Therefore, there was an overall increase in both ratios presumably due to surface contamination of the nano-catalyst with CO_x and/or H_2O in the atmosphere during sample preparation for analysis. This result confirms an earlier investigation with the FTIR spectrum for $TiO_2/PrSO_3H$ nano-catalyst. In addition, the percentage of sulphur to carbon atomic ratios using XPS quantitative analysis in $TiO_2/PrSO_3H$ nano-catalyst was 0.22. This is in agreements with the results obtained by CHNS analysis. In the case of TiO_2-NPs, the detailed high resolution XPS analysis demonstrated in our previous work [4].

Thermal stability analysis gave insights on the species evolved upon heating of the nano-catalyst that was prepared via surface grafting ($PrSO_3H$). Figure 10a shows the

weight loss of $TiO_2/PrSO_3H$ and initial TiO_2-NPs as determined by thermogravimetric analysis (TGA) under N_2 purge gas. There was a negligible weight loss from 25°C to 120°C for both samples assigned to desorption of H_2O/CO_x molecules from the surface of TiO_2. In the case of initial TiO_2-NPs, there was no further mass loss up to 900°C. In contrast, there was a gradual weight loss of about 2% from $TiO_2/PrSO_3H$ at 210°C to 500°C; afterwards there was no further weight loss up to 900°C. This is due to the thermal decomposition of $PrSO_3H$ species on the surface of TiO_2-NPs. This result agrees with results of the CHNS elemental analysis and is in accordance with the FTIR results. It must be noted also from the DSC results (see Figure 10b) that there is only one sharp distinct endothermic peak observed at 210°C with enthalpy of -60 mJ corresponding to the decomposition of $PrSO_3H$ groups on the surface of TiO_2-NPs. This is further evidence that the surface of TiO_2-NPs was successfully functionalised with PrO_3H groups.

Figure 11 illustrates that the surface grafting of TiO_2 with $PrSO_3H$ groups resulted in the position shift of all diffraction peaks to a bit higher 2θ angles by 0.2° indicating the decrease of the unit-cell sizes. Moreover, a reduction of intensity in all reflections is observed for $TiO_2/PrSO_3H$ as compared with the initial TiO_2-NPs precursor. Furthermore, the position of the main diffraction peaks with 100% intensity of initial TiO_2-NPs were observed at 2θ value of 25.3° corresponding to the [101] for 81.6% of tetragonal anatase phase structure (JCPDS-ICDD: 04-014-5762) whilst the peak at 2θ value of 27.43° assigned to the [110] for 18.4% of tetragonal rutile phase structure (JCPDS-ICDD: 01-072-41815). In the case of $TiO_2/PrSO_3H$ nano-catalyst, the XRD patterns matched all the diffraction peaks with tetragonal anatase phase (JCPDS-ICDD: 01-084-1286) and tetragonal rutile phase (JCPDS-ICDD: 01-072-4817).

However, no characteristic extra peak was observed for the $PrSO_3H$ groups, which suggested that these groups were only grafted on the surface of TiO_2-NPs, rather than impregnating the main crystallographic structure as expected. The detailed interlayer spacing values and calculated crystallite sizes of the [101] peak for anatase and [110] peak for rutile from the initial TiO_2-NPs and $PrSO_3H$ surface functionalized TiO_2-NPs are summarised in Table 2.

3.2 Catalytic performance

The catalytic activity of $TiO_2/PrSO_3H$ nano-catalyst for simultinous esterification and transesterification of UCO to produce biodiesel fuel was investigated. The effect of different reaction times, catalyst loadings, mole ratios of methanol to oil, and reaction temperatures on the percentage of FAME yields were studied and the results are presented in Figure 12. The reaction time of esterification/transesterification was varied between ½ hr and 9 hrs whilst other process parameters were kept constant at 1wt% of $TiO_2/PrSO_3H$ nano-catalyst to UCO feedstock, 6:1 methanol to oil mole ratio, 65°C reaction temperature, 600 RPM agitation rate, 0.14% moisture, and <2.0% of FFA content in raw material (UCO). It was found that the initial (trans)esterification reaction rate was very low, as shown in Figure 12 (a). This could possibly be due to the immiscibility of reactants (solid-liquid-liquid phases)/ the initial mass transfer limitations. The FAME yield further increased but was still lower than 10% FAME yield when the experiment was run for a longer time (9 hrs). This is because of the better micibility of reactants (solid acid nano-catalyst, methanol and UCO) with the time and increasing of mass transfer. The results of different catalyst to oil loadings on the FAME yield, however, shows the yield of FAME was almost doubled (see Figure 12(B)) when the (trans)esterification process was set at 9hrs of reaction time, 2wt% of nanocatalyst to UCO, 6:1 methanol to oil mole ratio, 65°C reaction temperature, 600 RPM of agitation rate, 0.14% moisture and <2.0% of FFA in raw material. This was attributed to the fact that the number of

active sites were increasing with an increase the catalyst concentration in the reaction system requiring a shorter time to reach the equalibrium [58]. Furthermore, the yield of FAME further increased from 14.92% to 38.7% with an increase in the nano-catalyst loading from 2wt% to 4.5wt% of UCO. Increasing the catalyst concentrations will lead to an increase in the number of active sites (proton, $-SO_3H$, concentration in the interface), which enhanced selectivity towards the FAME product [59].

A maximum conversion of FFA/triglycerides (TG) into FAME is required in simultinous esterification and transesterification reactions to obtain the highest yield of FAME in order to satisfy the EU and ASTM standards for obatined biodiesel fuel. In theory, the stoichiometric ratio for transesterification reaction requires three moles of methanol per mole of TG to obtain three moles of FAME and one mole of glycerol whilst this ratio is one to one for esterification reaction [60]. However, transesterification reaction practically needs an excess amount of methanol in order to get a complete conversion. In order to drive the reaction towards the highest FAME yield [61], various mole ratios of methanol to UCO were used [see Figure 12 (c)] under the aforementioned reaction conditions. It can be noted that the highest FAME yield of 98.1% was obtained when the mole ratio of methanol to UCO was steadily increased to 15:1 whilst the other parameters were fixed as most probably to a higher molar ratio of methanol to UCO leads to an increase of miscibility of reactants which shift the equalibrium to the product side and increase the probability of a methanol nucleophilic attack on the carbonyl/carboxylic acid functional groups in the FFA/TG. However, a further mole ratio of methanol to oil increase leads to a slight reduction in the FAME yield [58, 62], presumably as glycerol and FAME solubility in excess methanol can help to derive the reverse side of transesterification reaction [10].

The rate of esterification/transesterification reactions are strongly dependent on the process temperature. The effect of temperature on the FAME yield, whilst other parameters were set

at 9hrs reaction time, 4.5wt% of $TiO_2/PrSO_3H$ to UCO, 15:1 molar ratio of methanol to UCO, 600RPM agitation rate, 0.14% moisture content, and <2% of FFA content in UCO raw material, is shown in Figure 12 (D). It can be noted that the increase of reaction temperature from 25°C to 60°C led to smooth increase in the rate of the (trans)esterification process to reach 98.3% FAME yield. The reason for obtaining a high FAME yield at a higher temperature can be explained by the fact that the higher reaction temperature accelerates (1) the movement of molecules in reactants, (2) solubility of TG in methanol, (3) diffusion of TG molecules, as well as (4) generating more neucleophilic sites in the reaction system which results in an increase in reaction rate. This could help to initiate the activation of carboxylic/carbonyl function groups in FFA/TG by nucleophile [14]. Further studies on the reaction kinetic of the esterification/transesterification reaction using $TiO_2/PrSO_3H$ nano-catalyst should be reported in the future publications.

3.3 Catalytic activity and its reusability

The catalytic activity of $TiO_2/PrSO_3H$ nano-catalyst was assessed by the addition of different percentages of oleic acid in virgin oil because the presence of FFA in the feedstock has a great influence on the deactivation of catalysts. The addition of oleic acid in virgin oil was varied from 0.5% to 6% under determined optimium reaction conditions as reported in previous section. It can be observed from Figure 13(a), that the FAME yield was greatly reduced with an increase in the percentage of oleic acids in the virgin oil as raw material. This can be explained by the rate of esterification which was much faster than the transesterification [61] producing more water (by-product) in the reaction medium in a shorter time. The produced excess water in the reaction medium would probably deactivate the active sites of the catalyst. Likewise, the presence of a high concentration of oleic acid in the reaction medium leads to the rapid formation of ester and water (by-product). Produced

water from the reaction as a by-product may drive the reverse reaction to re-form FFA and methanol [63, 64].

The spent $TiO_2/PrSO_3H$ nano-catalyst was recovered from the reaction products and by-products at the end of each run by using centrifuge (Megafuge 16R, UK) and then properly washed several times with 1:1 ratio of methanol to n-hexane in order to remove any remaining impurities (polar and non-polar components) on its surface. The recycled catalyst was later dried in an oven for 3hrs at 110°C to remove any moisture on the surface prior to being re-used under optimised process conditions to investigate its remaining activity.

It was found that $TiO_2/PrSO_3H$ can be re-used up to four times under optimized reaction conditions, i.e. reaction temperature of 60°C, 4.5 wt% of $TiO_2/PrSO_3H$ nano-catalyst to UCO, molar ratios of methanol to UCO of 15:1, 600 RPM agitation rate, 0.14% moisture, <2.0% FFA, and 9hrs reaction time. However, thereafter, the yield of FAME was sharply reduced to 20.64%, as shown in Figure 13 (b). This obvious change in the production of FAME yield is due to the organic or carbonaceous materials on the surface of recycled nano-catalyst causing blockage of the active sites and/or detachment (leaching) of the $PrSO_3H$ species on the surface of TiO_2-NPs [65-68]. According to the XRD results shown in Figure 14, there was an accumulation of organic or carbonaceous materials from the surface of the prepared mesoporous solid acid nano-catalyst after four runs. This possibly inhibited the contact between the reactants and the active sites of the nano-catalyst [10, 40, 44, 66]. In order to fully understand the catalytic poisoning of the spent $TiO_2/PrSO_3H$ nano-catalyst, further studies should be carried out in detail, using the XPS, temperature programmed desorption (TPD)-MS, Hammett indicator titration, TEM-EDS, and CHNS techniques.

3.4 Biodiesel characterisations

The properties of obtained biodiesel are mainly dependent on the FAME compositions [17]. Therefore, off-line GC-MS was used to analyse the final product in order to quantify FAME content of synthesised biodiesel using $TiO_2/PrSO_3H$ solid acid nano-catalyst. The FAME compositions for obtained biodiesel are listed in Table 3.

It was found from Table 3 that the major FAMEs are palmitic acid methyl ester, stearic acid methyl ester, oleic acid methyl ester, linoleic acid methyl ester, linolenic acid methyl ester, and gadoleic acid methyl ester. The quality of final biodiesel fuel obtained under optimum reaction conditions are summarised in Table 4. The fuel properties of obtained biodiesel fuel were evaluated and the results revealed that the quality of produced biodiesel from the current study fulfilled ASTM and EU standards for biodiesel fuel quality control.

The cloud point is the temperature at which a cloud or few crystals form in a biodiesel fuel caused by the first stage of crystallisation on cooling of the fuel. It is one of the most important properties of biodiesel, which influences its use in a cold environment due to the possibility of causing fuel injector problems, poor fuel atomization, incomplete combustion, and deposit formation [17]. The DSC thermogram for as-synthesised biodiesel is shown in Figure 15. It can be seen from the cooling DSC curve that there is only one sharp endothermic peak centred at -11°C with enthalpy of 67.14mJ corresponding to the formation of crystals in biodiesel fuel. The onset temperature of crystallisation on the cooling curve at -10.57°C represents the cloud point temperature of prepared biodiesel. In heating DSC thermogram, a board exothermic peak was observed between -28°C and 0°C assigned to the melting of the formed crystals.

Thermal oxidative behaviour plays a key role in the industrial application of the biodiesel fuel [69]. The TGA thermogram for prepared biodiesel with onset and endset

temperatures are shown in Figure 16. The onset temperature (174°C) represent the biodiesel sample starting to decompose whilst the endset temperature (252°C) corresponds to the completely burnt off biodiesel sample. These results indicate that the synthesised biodiesel was thermally stable in atmosphere.

3.5 Discussion

A novel $TiO_2/PrSO_3H$ nano-catalyst was prepared through grafting of TiO_2-NPs with 1,3-propane sultone in dry toluene under reflux at 120°C for 72hrs. The application of such material as solid acid nano-catalyst is reported for the first time for biodiesel production from UCO. The synthesised solid acid nano-catalyst shows a remarkable catalytic activity for simultaneous esterification and transesterification of cheap feedstocks, probably due to the catalytic activity of such material according to its surface property ($-SO_3H$). It is important to mention that loading of higher density hydrophilic functional groups ($-SO_3H$) onto the surface of TiO_2-NPs may lead to an improvement in the hydrophilicity of TiO_2-NPs support and increase the accessibility of raw material (FFAs, triglycerides and methanol) in the simultaneous esterification and transesterification processes to the $–SO_3H$ groups. Therefore, more investigations could to be carried out in future on the effect of different TiO_2 phases (anatase, rutile and brookite) with different loadings of $PrSO_3H$ species and the surface acidity/strength of $TiO_2/PrSO_3H$ for the catalytic performance. Such future studies could fully utilize the potential of such nano-catalyst on the FAME yield produced from simultaneous esterification and transesterification of UCO. The prepared solid acid nano-catalyst was found to esterify FFA in cheap raw materials to FAME in parallel with transesterification of TG without formation of soaps. The nano-catalyst was also found to be a non-hazardous material compared to conventional homogenous acids and it can be used in four consecutive (trans)esterification cycles with no appreciable loss in catalytic activity,

which may satisfy the principle of green chemistry. Table 5 summarizes the comparison of the optimised process condition results for biodiesel production from UCO/oleic acid using solid acid catalyst in the present study with other reported solid acid catalysts in the literature.

4. CONCLUSIONS

Mesoporous $TiO_2/PrSO_3H$ solid acid nano-catalyst with an average particle size of around 23.1nm has been successfully synthesized as a novel inorganic–organic hybrid heterogeneous nano-catalyst from TiO_2-NPs and 1,3-propyl sulfonic acid for simultaneous esterification and transesterification of UCO containing FFA. STEM EELs-maps shows that the $PrSO_3H$ groups decorate the surface of TiO_2-NPs layer-by-layer. N_2 adsorption-desorption isotherms result demonstrated that surface modification reduced the surface area of TiO_2-NPs by 5% with an increase in the mean pore size and total pore volume. The XPS confirmed that the $PrSO_3H$ functional groups attached to the surface of TiO_2-NPs. $TiO_2/PrSO_3H$ nano-catalyst performance showed promising results for catalytic simultaneous esterification and transesterification of cheap raw materials for biodiesel production. The enhanced catalytic performance mainly relates to the loading of propyl sulfonic acid groups on the surface of TiO_2-NPs.

ACKNOWLEDGEMENT

This study was funding by the Human Capacity Development Program (HCPD) of the Kurdistan Regional Government (KRG) for one of our authors (JG). Discussions with Professor Karen Wilson at the European Bioenergy Research Institute (EBRI) was highly valuable for this study. We are thankful to Dr Adrian Cunliffe, Dr Mike Ward and Dr Faye Esat for their technical assistance.

REFERENCES

1. Shen, J., Y. Zhu, X. Yang, and C. Li, *Magnetic composite microspheres with exposed {001} faceted TiO_2 shells: a highly active and selective visible-light photocatalyst.* Journal of Materials Chemistry, **2012**. 22(26): p. 13341-13347.
2. Rehan, M., X. Lai, and G.M. Kale, *Hydrothermal synthesis of titanium dioxide nanoparticles studied employing in situ energy dispersive X-ray diffraction.* CrystEngComm, **2011**. 13(11): p. 3725-3732.
3. Patsoura, A., D.I. Kondarides, and X.E. Verykios, *Enhancement of photoinduced hydrogen production from irradiated Pt/TiO_2 suspensions with simultaneous degradation of azo-dyes.* Applied Catalysis B: Environmental, **2006**. 64(3): p. 171-179.
4. Gardy, J., A. Hassanpour, X. Lai, and M.H. Ahmed, *Synthesis of $Ti(SO_4)O$ solid acid nano-catalyst and its application for biodiesel production from used cooking oil.* Applied Catalysis A: General, **2016**. 527: p. 81–95.
5. Ahmed, M.H., J.A. Byrne, and T.E. Keyes, *Investigation of the inhibitory effects of TiO_2 on the β-amyloid peptide aggregation.* Materials Science and Engineering: C, **2014**. 39: p. 227-234.
6. Bourikas, K., M. Stylidi, D.I. Kondarides, and X.E. Verykios, *Adsorption of acid orange 7 on the surface of titanium dioxide.* Langmuir, **2005**. 21(20): p. 9222-9230.
7. Hanaor, D.A. and C.C. Sorrell, *Review of the anatase to rutile phase transformation.* Journal of Materials science, **2011**. 46(4): p. 855-874.
8. Kang, S., J. Ye, and J. Chang, *Recent advances in carbon-based sulfonated catalyst: preparation and application.* International Review of Chemical Engineering (IRECHE), **2013**. 5(2): p. 133-144.
9. Patel, A. and V. Brahmkhatri, *Kinetic study of oleic acid esterification over 12-tungstophosphoric acid catalyst anchored to different mesoporous silica supports.* Fuel processing technology, **2013**. 113: p. 141-149.
10. Melero, J.A., L.F. Bautista, G. Morales, J. Iglesias, and R. Sánchez-Vázquez, *Biodiesel production from crude palm oil using sulfonic acid-modified mesostructured catalysts.* Chemical Engineering Journal, **2010**. 161(3): p. 323-331.
11. Toh-Ae, P., B. Junhasavasdikul, N. Lopattananon, and K. Sahakaro. *Surface modification of TiO_2 nanoparticles by grafting with silane coupling agent*. in *Advanced Materials Research*. **2014**. Trans Tech Publ.
12. Zhao, J., M. Milanova, M.M. Warmoeskerken, and V. Dutschk, *Surface modification of TiO_2 nanoparticles with silane coupling agents.* Colloids and surfaces A: Physicochemical and engineering aspects, **2012**. 413: p. 273-279.
13. Radoman, T., J. Džunuzović, K. Trifković, T. Palija, A. Marinković, B. Bugarski, and E. Dſunuzović, *Effect of surface modified TiO_2 nanoparticles on thermal, barrier and mechanical properties of long oil alkyd resin-based coatings.* Express Polymer Letters, **2015**. 9(10).
14. Shu, Q., J. Gao, Z. Nawaz, Y. Liao, D. Wang, and J. Wang, *Synthesis of biodiesel from waste vegetable oil with large amounts of free fatty acids using a carbon-based solid acid catalyst.* Applied Energy, **2010**. 87(8): p. 2589-2596.
15. Lee, A.F. and K. Wilson, *Recent developments in heterogeneous catalysis for the sustainable production of biodiesel.* Catalysis Today, **2015**. 242: p. 3-18.
16. Alhassan, F.H., U. Rashid, and Y. Taufiq-Yap, *Synthesis of waste cooking oil-based biodiesel via effectual recyclable bi-functional Fe_2O_3-MnO-SO_4^{2-}/ZrO_2 nanoparticle solid catalyst.* Fuel, **2015**. 142: p. 38-45.

17. Gardy, J., A. Hassanpourm, X. Lai, A. Cunliffe, and M. Rehan, *The influence of blending process on the quality of rapeseed oil-used cooking oil biodiesels.* Int. Sci. J. Environ. Sci, **2014**. 3: p. 233-240.
18. Nizami, A., O. Ouda, M. Rehan, A. El-Maghraby, J. Gardy, A. Hassanpour, S. Kumar, and I. Ismail, *The potential of Saudi Arabian natural zeolites in energy recovery technologies.* Energy, **2015**.
19. Wang, H., J. Covarrubias, H. Prock, X. Wu, D. Wang, and S.H. Bossmann, *Acid-functionalized magnetic nanoparticle as heterogeneous catalysts for biodiesel synthesis.* The Journal of Physical Chemistry C, **2015**. 119(46): p. 26020-26028.
20. Atabani, A.E., A.S. Silitonga, I.A. Badruddin, T. Mahlia, H. Masjuki, and S. Mekhilef, *A comprehensive review on biodiesel as an alternative energy resource and its characteristics.* Renewable and sustainable energy reviews, **2012**. 16(4): p. 2070-2093.
21. Sani, Y.M., W.M.A.W. Daud, and A.A. Aziz, *Activity of solid acid catalysts for biodiesel production: a critical review.* Applied Catalysis A: General, **2014**. 470: p. 140-161.
22. Refaat, A., *Biodiesel production using solid metal oxide catalysts.* International Journal of Environmental Science & Technology, **2011**. 8(1): p. 203-221.
23. Gong, S.-w., J. Lu, H.-h. Wang, L.-j. Liu, and Q. Zhang, *Biodiesel production via esterification of oleic acid catalyzed by picolinic acid modified 12-tungstophosphoric acid.* Applied Energy, **2014**. 134: p. 283-289.
24. Lee, A.F., *Catalysing sustainable fuel and chemical synthesis.* Applied Petrochemical Research, **2014**. 4(1): p. 11-31.
25. Melero, J.A., J. Iglesias, and G. Morales, *Heterogeneous acid catalysts for biodiesel production: current status and future challenges.* Green Chemistry, **2009**. 11(9): p. 1285-1308.
26. Kango, S., S. Kalia, A. Celli, J. Njuguna, Y. Habibi, and R. Kumar, *Surface modification of inorganic nanoparticles for development of organic–inorganic nanocomposites—a review.* Progress in Polymer Science, **2013**. 38(8): p. 1232-1261.
27. Laurent, S., D. Forge, M. Port, A. Roch, C. Robic, L. Vander Elst, and R.N. Muller, *Magnetic iron oxide nanoparticles: synthesis, stabilization, vectorization, physicochemical characterizations, and biological applications.* Chemical reviews, **2008**. 108(6): p. 2064-2110.
28. Atghia, S. and S.S. Beigbaghlou, *Nanocrystalline titania-based sulfonic acid (TiO_2-Pr-SO_3H) as a new, highly efficient and recyclable solid acid catalyst for the N-Boc protection of amines at room temperature.* Journal of Organometallic Chemistry, **2013**. 745: p. 42-49.
29. Mo, X., D.E. López, K. Suwannakarn, Y. Liu, E. Lotero, J.G. Goodwin, and C. Lu, *Activation and deactivation characteristics of sulfonated carbon catalysts.* Journal of Catalysis, **2008**. 254(2): p. 332-338.
30. Ahn, B.K., H. Wang, S. Robinson, T.B. Shrestha, D.L. Troyer, S.H. Bossmann, and X.S. Sun, *Ring opening of epoxidized methyl oleate using a novel acid-functionalized iron nanoparticle catalyst.* Green chemistry, **2012**. 14(1): p. 136-142.
31. Melero, J.A., L.F. Bautista, J. Iglesias, G. Morales, R. Sánchez-Vázquez, and I. Suárez-Marcos, *Biodiesel production over arenesulfonic acid-modified mesostructured catalysts: optimization of reaction parameters using response surface methodology.* Topics in Catalysis, **2010**. 53(11-12): p. 795-804.
32. Li, W.L., S.B. Tian, and F. Zhu, *Sulfonic acid functionalized nano-γ-Al_2O_3: A new, efficient, and reusable catalyst for synthesis of 3-substituted-2h-1, 4-benzothiazines.* The Scientific World Journal, **2013**. 2013.

33. Yang, L., Y. Wang, G. Luo, and Y. Dai, *Functionalization of SBA-15 mesoporous silica with thiol or sulfonic acid groups under the crystallization conditions.* Microporous and mesoporous materials, **2005**. 84(1): p. 275-282.
34. Díaz, I., C. Márquez-Alvarez, F. Mohino, J.n. Pérez-Pariente, and E. Sastre, *Combined alkyl and sulfonic acid functionalization of MCM-41-type silica: Part 2. Esterification of glycerol with fatty acids.* Journal of Catalysis, **2000**. 193(2): p. 295-302.
35. Melero, J.A., R. van Grieken, and G. Morales, *Advances in the synthesis and catalytic applications of organosulfonic-functionalized mesostructured materials.* Chemical reviews, **2006**. 106(9): p. 3790-3812.
36. Alvaro, M., A. Corma, D. Das, V. Fornés, and H. García, *"Nafion"-functionalized mesoporous MCM-41 silica shows high activity and selectivity for carboxylic acid esterification and Friedel–Crafts acylation reactions.* journal of Catalysis, **2005**. 231(1): p. 48-55.
37. Pirez, C., M.T. Reche, A. Lee, J. Manayil, V. dos-Santos, and K. Wilson, *Hydrothermal saline promoted grafting of periodic mesoporous organic sulfonic acid silicas for sustainable FAME production.* Catalysis Letters, **2015**. 145(7): p. 1483-1490.
38. Sobhani, S., Z.P. Parizi, and N. Razavi, *Nano n-propylsulfonated γ-Fe_2O_3 as magnetically recyclable heterogeneous catalyst for the efficient synthesis of β-phosphonomalonates.* Applied Catalysis A: General, **2011**. 409: p. 162-166.
39. Margolese, D., J. Melero, S. Christiansen, B. Chmelka, and G. Stucky, *Direct syntheses of ordered SBA-15 mesoporous silica containing sulfonic acid groups.* Chemistry of Materials, **2000**. 12(8): p. 2448-2459.
40. Zuo, D., J. Lane, D. Culy, M. Schultz, A. Pullar, and M. Waxman, *Sulfonic acid functionalized mesoporous SBA-15 catalysts for biodiesel production.* Applied Catalysis B: Environmental, **2013**. 129: p. 342-350.
41. Mbaraka, I.K., K.J. McGuire, and B.H. Shanks, *Acidic mesoporous silica for the catalytic conversion of fatty acids in beef tallow.* Industrial & engineering chemistry research, **2006**. 45(9): p. 3022-3028.
42. Basaldella, E.I., M.S. Legnoverde, I. Jiménez-Morales, E. Rodríguez-Castellón, B.O. Dalla Costa, and C.A. Querini, *Preparation, characterization and catalytic activity towards green reactions of sulfonic functionalized SBA-15.* Adsorption, **2011**. 17(3): p. 631-641.
43. Lotero, E., J.G. Goodwin Jr, D.A. Bruce, K. Suwannakarn, Y. Liu, and D.E. Lopez, *The catalysis of biodiesel synthesis.* catalysis, **2006**. 19(1): p. 41-83.
44. Melero, J.A., L.F. Bautista, J. Iglesias, G. Morales, R. Sánchez-Vázquez, K. Wilson, and A.F. Lee, *New insights in the deactivation of sulfonic modified SBA-15 catalysts for biodiesel production from low-grade oleaginous feedstock.* Applied Catalysis A: General, **2014**. 488: p. 111-118.
45. Bahnemann, D., A. Henglein, and L. Spanhel, *Detection of the intermediates of colloidal TiO_2-catalysed photoreactions.* Faraday Discussions of the Chemical Society, **1984**. 78: p. 151-163.
46. Soler-Illia, G.d.A., A. Louis, and C. Sanchez, *Synthesis and characterization of mesostructured titania-based materials through evaporation-induced self-assembly.* Chemistry of Materials, **2002**. 14(2): p. 750-759.
47. Pavia, D.L., G.M. Lampman, G.S. Kriz, and J.A. Vyvyan, *Introduction to spectroscopy*. **2008**: Cengage Learning.
48. Sirsam, R. and G. Usmani, *Preparation and characterization of sulfonic acid functionalized silica and its application for the esterification of ethanol and maleic Acid.* Journal of The Institution of Engineers (India): Series E, **2016**. 97(1): p. 75-80.

49. Muthirulan, P., C.N. Devi, and M.M. Sundaram, *TiO_2 wrapped graphene as a high performance photocatalyst for acid orange 7 dye degradation under solar/UV light irradiations.* Ceramics International, **2014**. 40(4): p. 5945-5957.
50. Lu, A.H., E.e.L. Salabas, and F. Schüth, *Magnetic nanoparticles: synthesis, protection, functionalization, and application.* Angewandte Chemie International Edition, **2007**. 46(8): p. 1222-1244.
51. Klobes, P., K. Meyer, and R.G. Munro, *Porosity and specific surface area measurements for solid materials.* **2006**.
52. Lam, M.K., K.T. Lee, and A.R. Mohamed, *Sulfated tin oxide as solid superacid catalyst for transesterification of waste cooking oil: an optimization study.* Applied Catalysis B: Environmental, **2009**. 93(1): p. 134-139.
53. Barroso-Bujans, F., J. Fierro, S. Rojas, S. Sánchez-Cortes, M. Arroyo, and M. López-Manchado, *Degree of functionalization of carbon nanofibers with benzenesulfonic groups in an acid medium.* Carbon, **2007**. 45(8): p. 1669-1678.
54. Hueso, J., J. Espinós, A. Caballero, J. Cotrino, and A. González-Elipe, *XPS investigation of the reaction of carbon with NO, O_2, N_2 and H_2O plasmas.* Carbon, **2007**. 45(1): p. 89-96.
55. Chastain, J., R.C. King, and J. Moulder, *Handbook of X-ray photoelectron spectroscopy: a reference book of standard spectra for identification and interpretation of XPS data*. **1995**: Physical Electronics Eden Prairie, MN.
56. Wu, L., Y. Zhou, W. Nie, L. Song, and P. Chen, *Synthesis of highly monodispersed teardrop-shaped core–shell SiO_2/TiO_2 nanoparticles and their photocatalytic activities.* Applied Surface Science, **2015**. 351: p. 320-326.
57. Yadav, H.M., S.V. Otari, V.B. Koli, S.S. Mali, C.K. Hong, S.H. Pawar, and S.D. Delekar, *Preparation and characterization of copper-doped anatase TiO_2 nanoparticles with visible light photocatalytic antibacterial activity.* Journal of Photochemistry and Photobiology A: Chemistry, **2014**. 280: p. 32-38.
58. Li, Y., S. Lian, D. Tong, R. Song, W. Yang, Y. Fan, R. Qing, and C. Hu, *One-step production of biodiesel from Nannochloropsis sp. on solid base Mg–Zr catalyst.* Applied energy, **2011**. 88(10): p. 3313-3317.
59. Shu, Q., Q. Zhang, G. Xu, Z. Nawaz, D. Wang, and J. Wang, *Synthesis of biodiesel from cottonseed oil and methanol using a carbon-based solid acid catalyst.* Fuel Processing Technology, **2009**. 90(7): p. 1002-1008.
60. Li, J., X. Wang, W. Zhu, and F. Cao, *$Zn_{1.2}H_{0.6}PW_{12}O_{40}$ nanotubes with double acid sites as heterogeneous catalysts for the production of biodiesel from waste cooking oil.* ChemSusChem, **2009**. 2(2): p. 177-183.
61. Kulkarni, M.G., R. Gopinath, L.C. Meher, and A.K. Dalai, *Solid acid catalyzed biodiesel production by simultaneous esterification and transesterification.* Green Chemistry, **2006**. 8(12): p. 1056-1062.
62. Teng, G., L. Gao, G. Xiao, and H. Liu, *Transesterification of soybean oil to biodiesel over heterogeneous solid base catalyst.* Energy & Fuels, **2009**. 23(9): p. 4630-4634.
63. Rattanaphra, D., A. Harvey, and P. Srinophakun, *Simultaneous conversion of triglyceride/free fatty acid mixtures into biodiesel using sulfated zirconia.* Topics in Catalysis, **2010**. 53(11-12): p. 773-782.
64. Morales, G., L.F. Bautista, J.A. Melero, J. Iglesias, and R. Sánchez-Vázquez, *Low-grade oils and fats: effect of several impurities on biodiesel production over sulfonic acid heterogeneous catalysts.* Bioresource technology, **2011**. 102(20): p. 9571-9578.
65. Xie, W. and C. Zhang, *Propylsulfonic and arenesulfonic functionalized SBA-15 silica as an efficient and reusable catalyst for the acidolysis of soybean oil with medium-chain fatty acids.* Food Chemistry, **2016**. 211: p. 74-82.

66. Lopez, D.E., J.G. Goodwin, D.A. Bruce, and E. Lotero, *Transesterification of triacetin with methanol on solid acid and base catalysts.* Applied Catalysis A: General, **2005**. 295(2): p. 97-105.
67. Jitputti, J., B. Kitiyanan, P. Rangsunvigit, K. Bunyakiat, L. Attanatho, and P. Jenvanitpanjakul, *Transesterification of crude palm kernel oil and crude coconut oil by different solid catalysts.* Chemical Engineering Journal, **2006**. 116(1): p. 61-66.
68. Mo, X., E. Lotero, C. Lu, Y. Liu, and J.G. Goodwin, *A novel sulfonated carbon composite solid acid catalyst for biodiesel synthesis.* Catalysis Letters, **2008**. 123(1-2): p. 1-6.
69. Xu, Y. and M.A. Hanna, *Synthesis and characterization of hazelnut oil-based biodiesel.* Industrial crops and products, **2009**. 29(2): p. 473-479.
70. Fu, X.-b., J. Chen, X.-l. Song, Y.-m. Zhang, Y. Zhu, J. Yang, and C.-w. Zhang, *Biodiesel production using a carbon solid acid catalyst derived from β-cyclodextrin.* Journal of the American Oil Chemists' Society, **2015**. 92(4): p. 495-502.
71. Feyzi, M., L. Nourozi, and M. Zakarianezhad, *Preparation and characterization of magnetic $CsH_2PW_{12}O_{40}/Fe–SiO_2$ nanocatalysts for biodiesel production.* Materials Research Bulletin, **2014**. 60: p. 412-420.

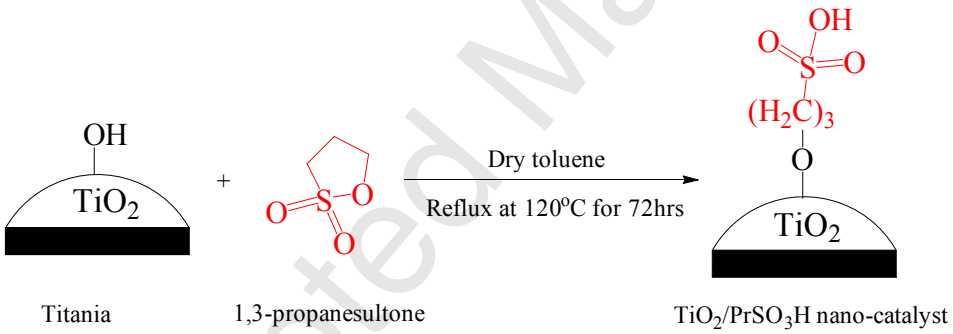

Titania 1,3-propanesultone $TiO_2/PrSO_3H$ nano-catalyst

Scheme 1: General proposed protocol for the synthesis of $TiO_2/PrSO_3H$ nano-catalyst

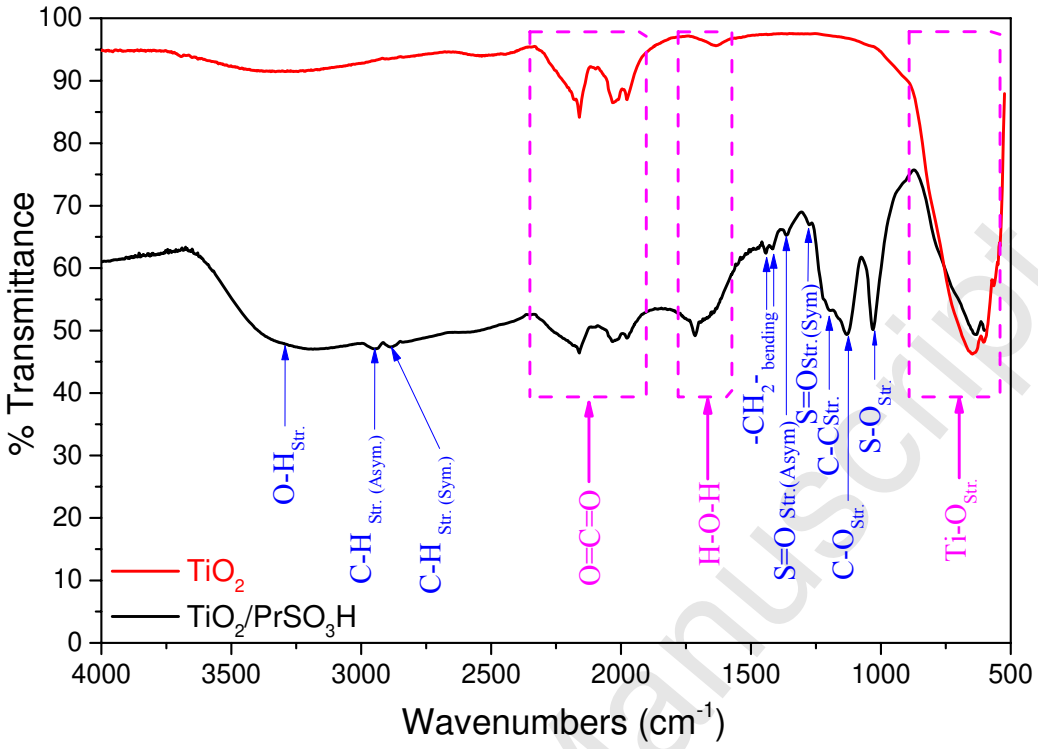

Figure (1): FT-IR spectra of $TiO_2/PrSO_3H$ (in black) and TiO_2 (in red) nano-catalysts

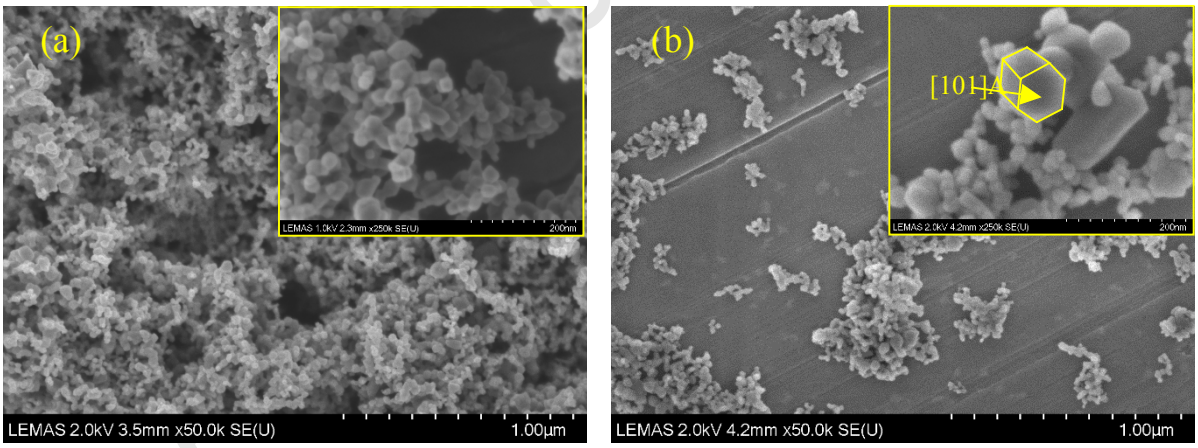

Figure (2): SEM images showing particle size and morphology distributions of (a) TiO_2 and (b) synthesised $TiO_2/PrSO_3H$ nano-catalyst

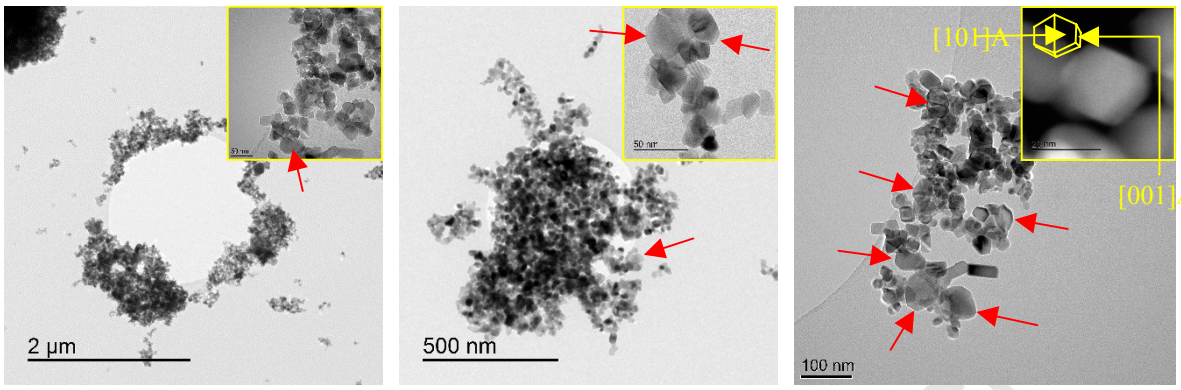

Figure (3): TEM images at different magnifications of synthesised $TiO_2/PrSO_3H$ nano-catalyst

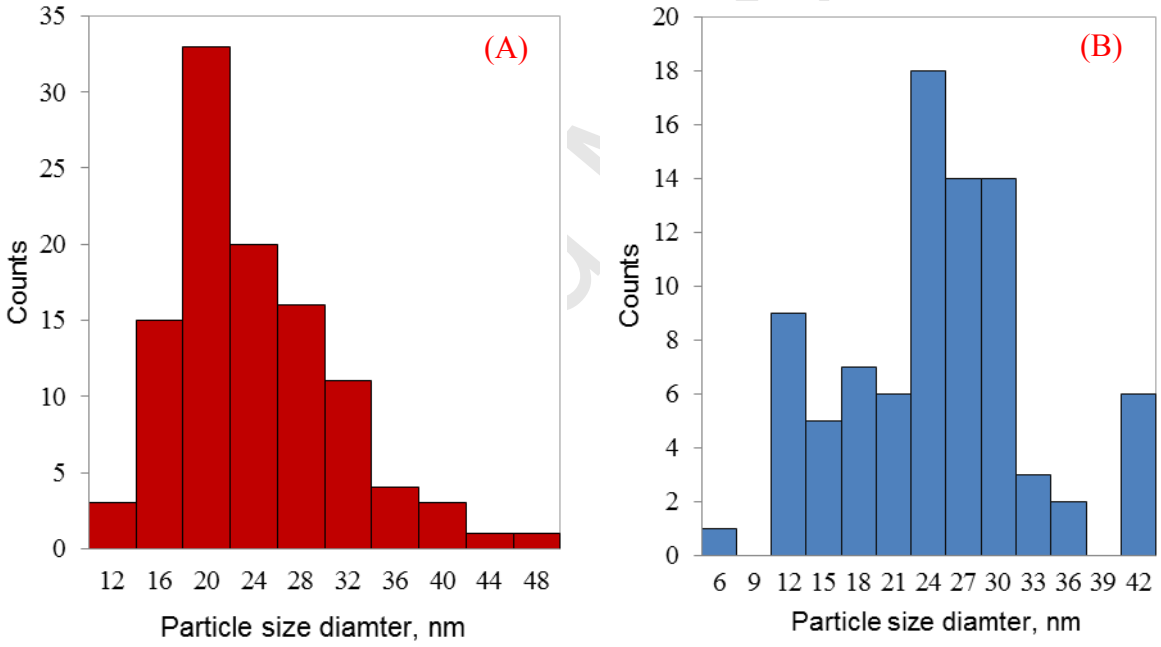

Figure (4): Particle size distributions for (a) TiO_2 and (b) $TiO_2/PrSO_3H$ nano-catalysts

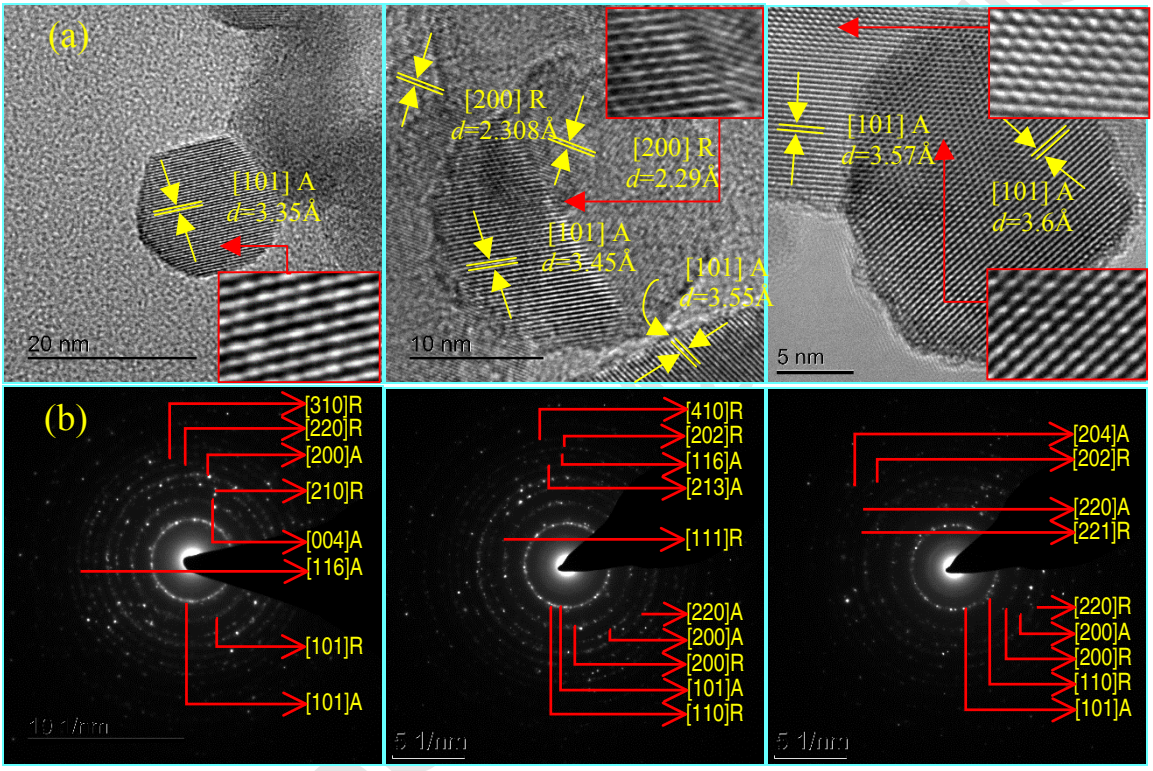

Figure (5): (a) High resolution TEM (HRTEM) micrograph images and (b) selected area electron diffraction (SAED) patterns for $TiO_2/PrSO_3H$ nano-catalyst

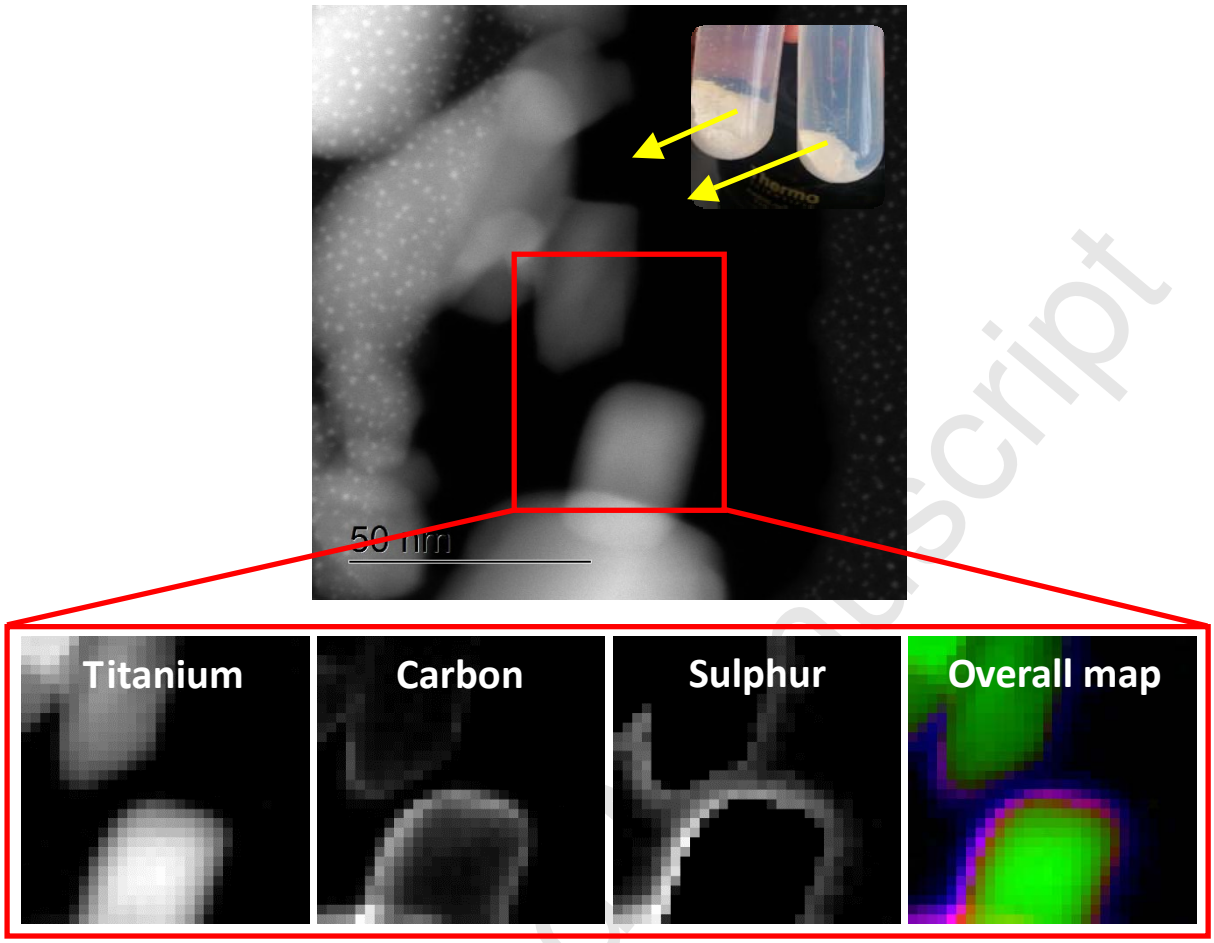

Figure (6): STEM image with EELs-mapping of synthesised $TiO_2/PrSO_3H$ nano-catalyst obtained from Titan at 300kV illustrating the 2D elemental mapping with high quality overall map of $TiO_2/PrSO_3H$ particles with the distribution of individual elements (Titanium in green, Carbon in violet, and Sulphur in blue).

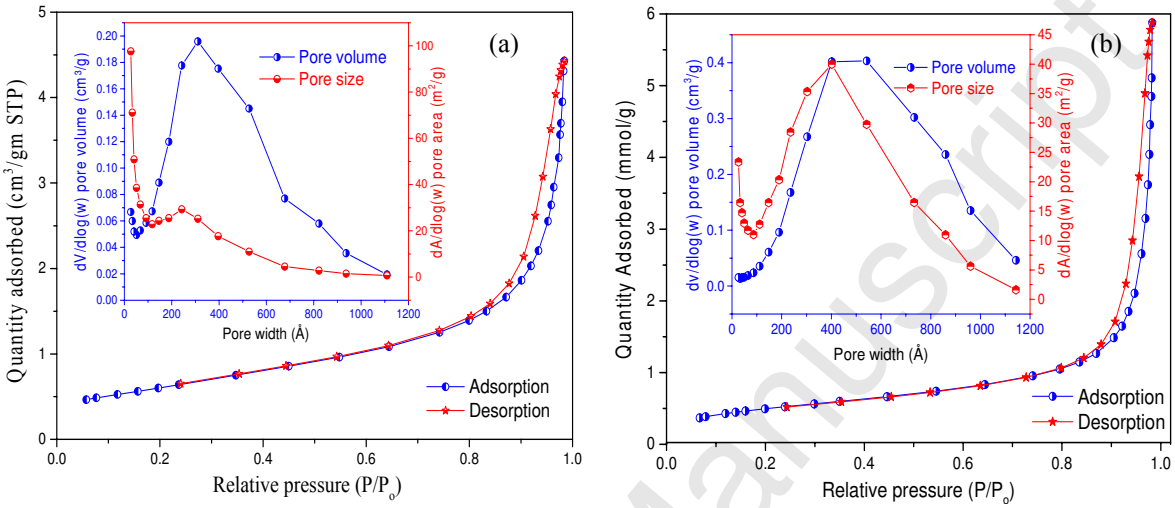

Figure (7): N_2 adsorption-desorption isotherms and total pore volumes with mean pore sizes (inset) for (a) TiO_2-NPs and (b) synthesised $TiO_2/PrSO_3H$ nano-catalysts.

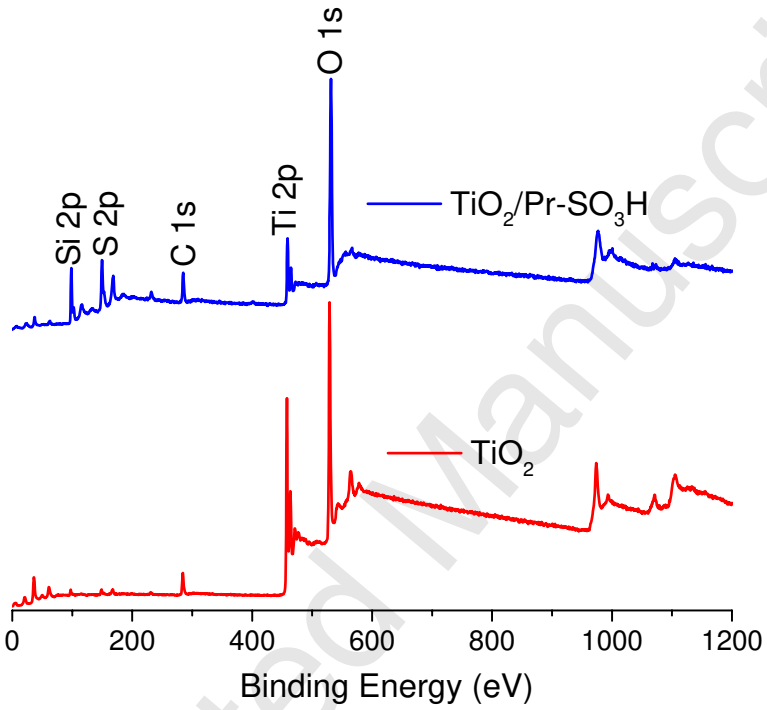

Figure (8): XPS survey scan of TiO_2-NPs and synthesised $TiO_2/PrSO_3H$ nano-catalysts

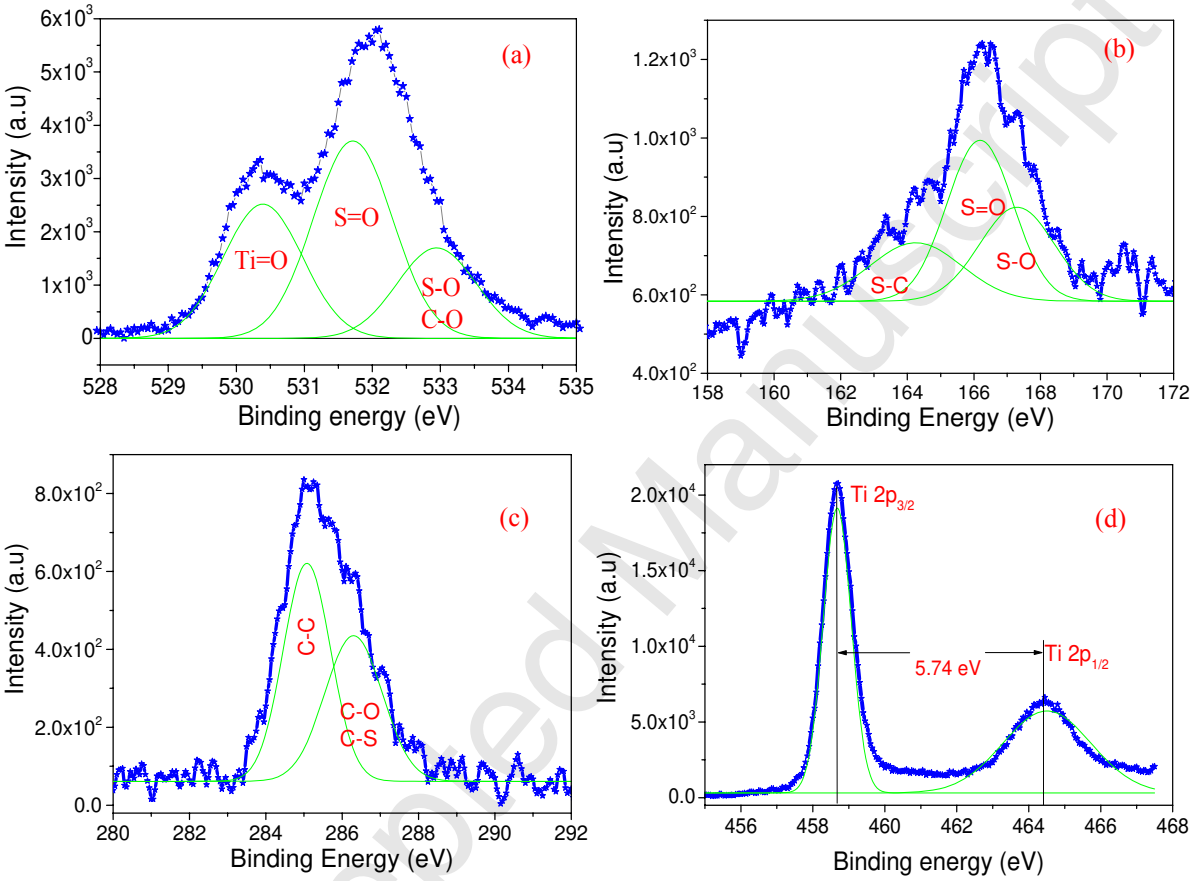

Figure (9): XPS spectra showing the chemical environments of (a) O 1s, (b) S 2p, (c) C 1s, and (d) the de-convolution of Ti 2p peaks in $TiO_2/PrSO_3H$ nano-catalyst

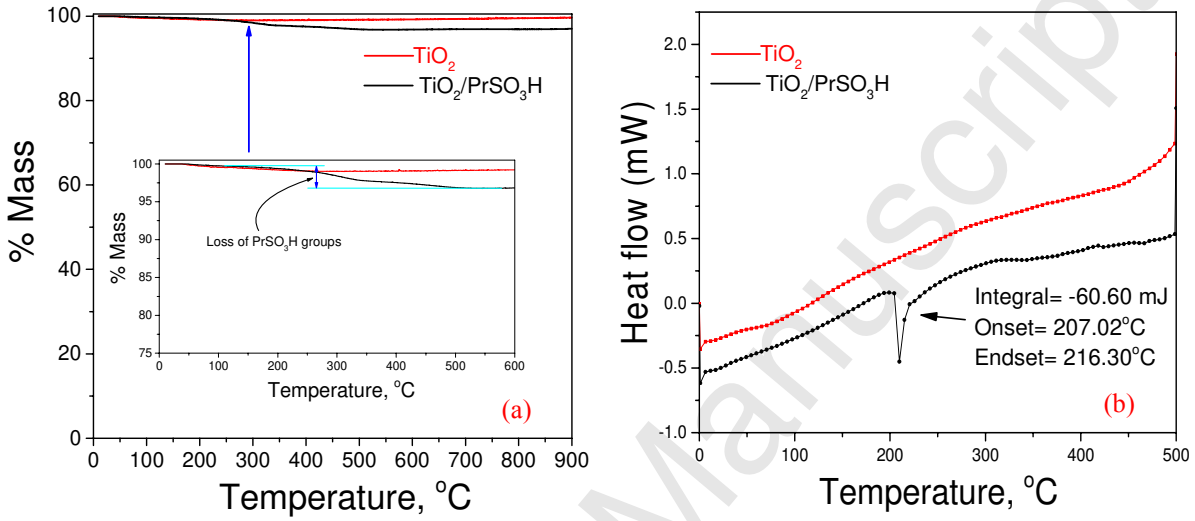

Figure (10): TGA (a) and DSC (b) profiles for TiO_2.and $TiO_2/PrSO_3H$ nano-catalysts

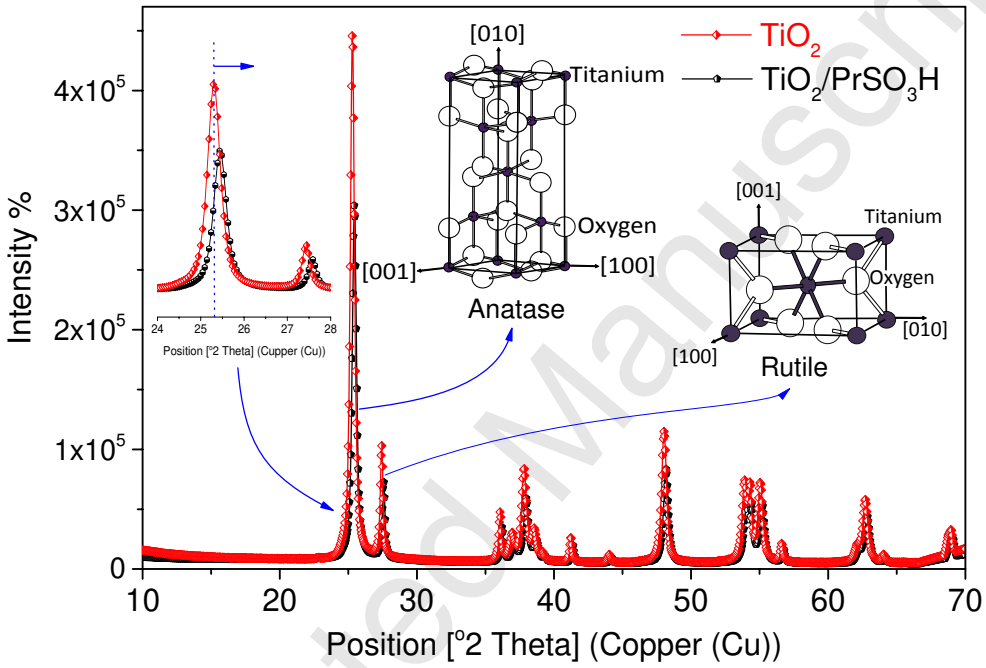

Figure (11): Powder XRD profiles for TiO_2 and $TiO_2/PrSO_3H$ nano-catalysts at RT.

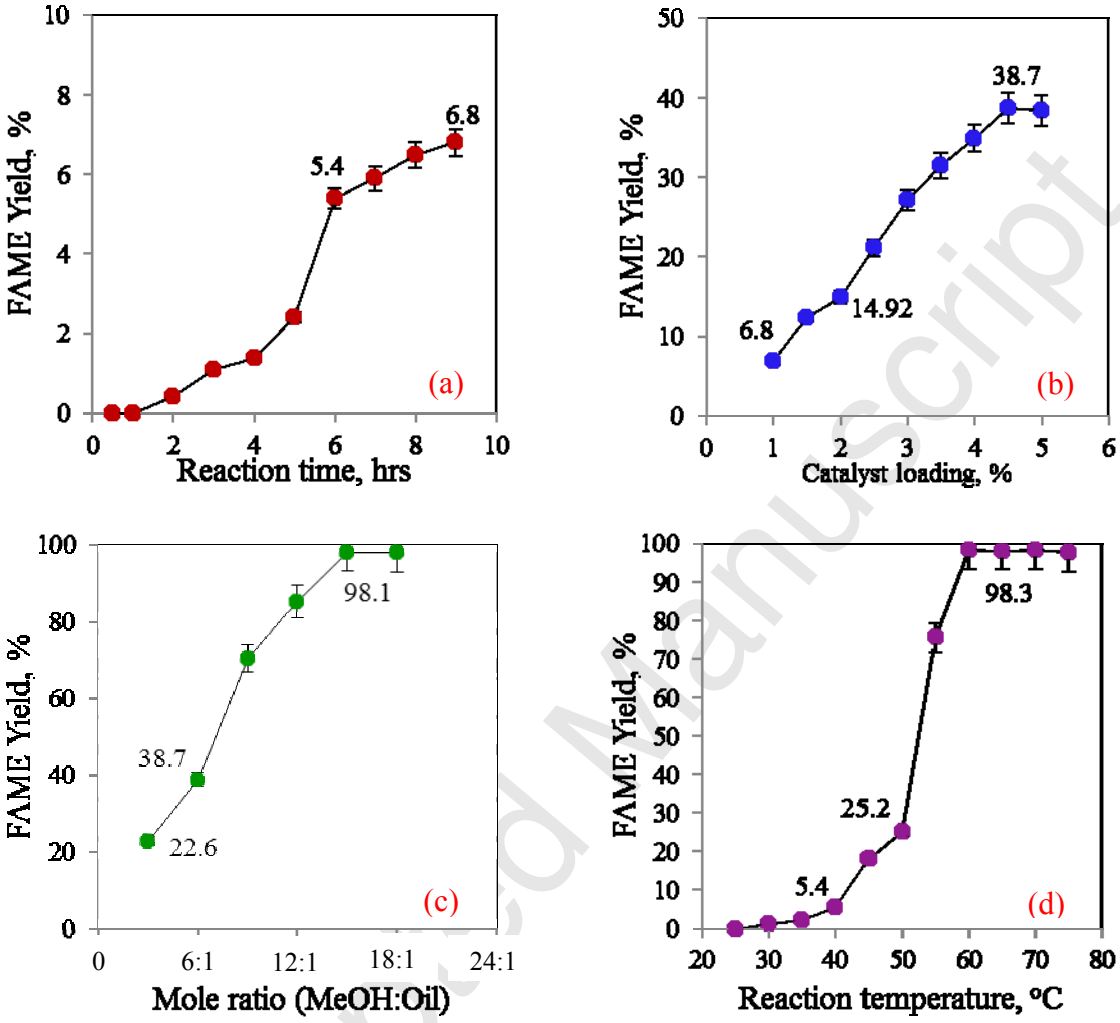

Figure (12): The effects of (a) reaction time, (b) $TiO_2/PrSO_3H$ nano-catalyst loading to UCO, (c) mole ratio of methanol to UCO, and (d) reaction temperature on the percentage of FAME yield.

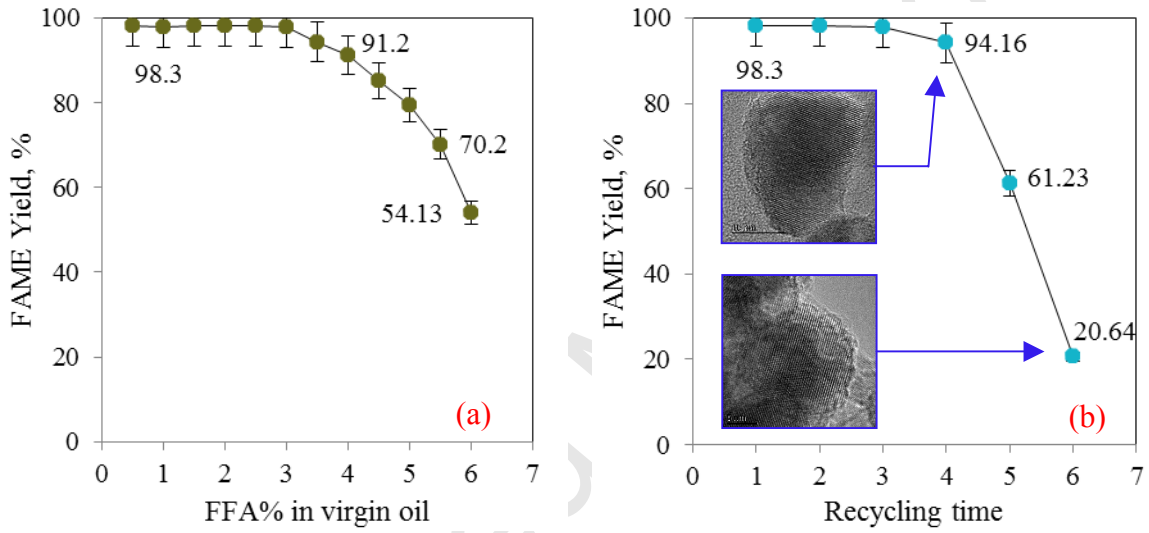

Figure (13): The effect of different concentration oleic acid addition in virgin oil (a) and reusability of $TiO_2/PrSO_3H$ nano-catalyst (b) on the percentage of FAME yield.

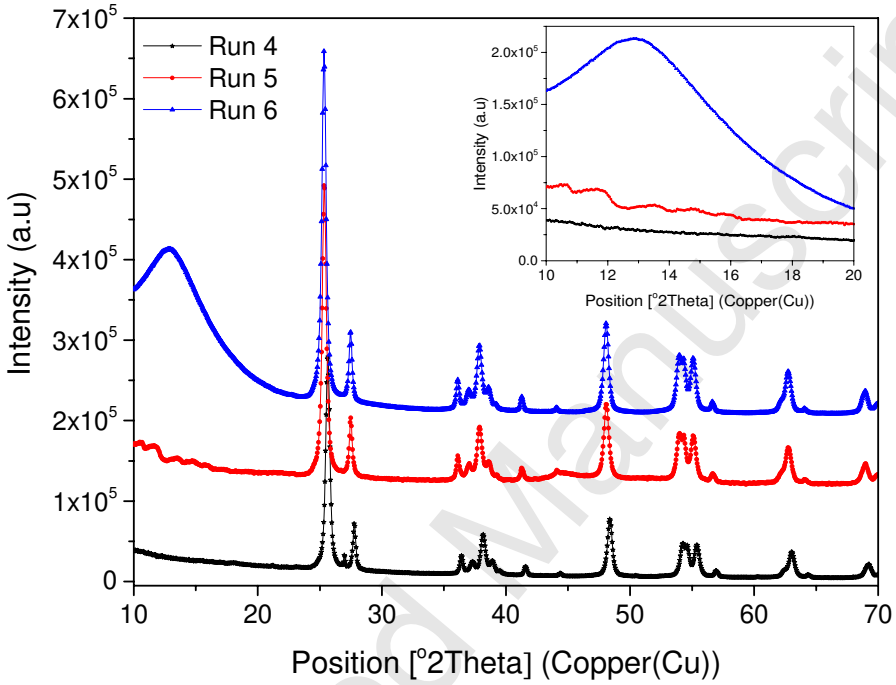

Figure (14) Powder XRD patterns of spent $TiO_2/PrSO_3H$ nano-catalyst for run 4 to run 6

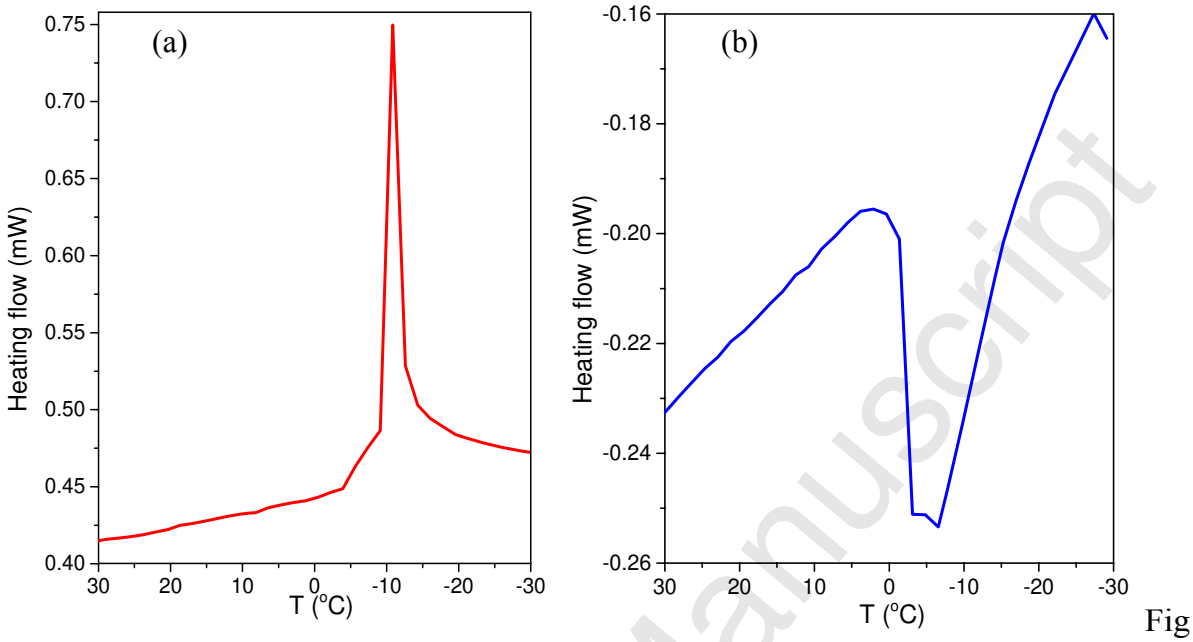

Figure (15): The DSC (a) cooling and (b) heating curves for obtained biodiesel

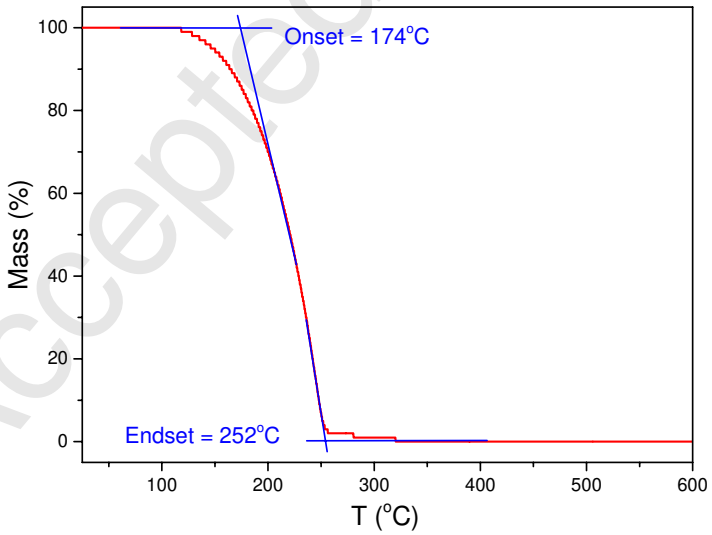

Figure (16): Typical TGA thermogram of obtained biodiesel in air

Table 1: Physicochemical parameters of $TiO_2/PrSO_3H$ nano-catalyst

	Texture properties [a]			CHNS analysis [b]		TEM-EDS [c]
	S_{BET}	V_p	D_p	C%	S%	S%
$TiO_2/PrSO_3H$	38.59	0.192	24.55	1.41	0.28	0.26

[a] S_{BET}: BET surface area ($m^2.g^{-1}$) calculated over the relative pressure range 0.05–0.2, D_p: Mean pore size (nm) calculated by applying the BJH model from N_2 desorption isotherm; V_p: Total pore volume ($cm^3.g^{-1}$) was determined at P/P_o =0.98. [b] C%: Carbon%, and S%: Sulphur% determined by using elemental (CHNS) analysis. The overall of sulphur loading on the surface of TiO_2-NPs was quantified using TEM-EDS analysis at different TEM spots.

Table 2: Comparison of *d*-spacing and crystallite sizes of TiO_2 and $TiO_2/PrSO_3H$

Sample	XRD peak	°2θ	FWHM	*d*-spacing, Å	D [*], nm
TiO_2	[101] Anatase	25.30	0.39	3.52	20.87
	[110] Rutile	27.43	3.26	3.25	2.51
$TiO_2/PrSO_3H$	[101] Anatase	25.47	0.41	3.49	19.86
	[110] Rutile	27.52	3.26	3.24	2.51

[*] D: The crystallite size of the 100% relative intensities XRD main peaks for anatase and rutile phases in nano-catalysts were estimated using Debye-Scherrer's formula [4].

Table 3: FAME profiles for as-prepared biodiesel from UCO

Name		% FAME
Myristic acid methyl ester	$C_{14:0}$	0.07
Palmitic acid methyl ester	$C_{16:0}$	7.86
Palmitoleic acid methyl ester	$C_{16:1}$	0.01
Stearic acid methyl ester	$C_{18:0}$	3.08
Oleic acid methyl ester	$C_{18:1}$	56.19
Linoleic acid methyl ester	$C_{18:2}$	26.74
Linolenic acid methyl ester	$C_{18:3}$	3.30
Arachidic acid methyl ester	$C_{20:0}$	0.00
Gadoleic acid methyl ester	$C_{20:1}$	1.32
Eicosadienoic acid methyl ester	$C_{21:0}$	0.10
Behenic acid methyl ester	$C_{22:0}$	0.43
Erucic acid methyl ester	$C_{22:1}$	0.64
Lignoceric acid methyl ester	$C_{24:0}$	0.12
Nervonic acid methyl ester	$C_{24:1}$	0.14

Table (4): Properties of UCO and obtained biodiesel over $TiO_2/PrSO_3H$ nano-catalyst

Property	Unit	Limits		UCO	Synthesised biodiesel
		ASTM D6751	EN14214		
Flash point	°C	93 min	101 min	289	171
Kinematic viscosity	mm^2/s	1.9-6.0	3.5-5.0	32. 91	4.8
Acid number	mgKOH/g	0.8 max	0.5 max	4.04	0.41
FFA	mass%	---	---	2.034	0.21
Density at 15°C	Kg/m^3	---	860-900	921	898.1
FAME content	% mass	---	96.5 min	0.00	98.3

Table 5 A mild process conditions for the production of biodiesel in the simultaneous esterification and transesterification from the current work compared to the reported solid acid catalysts

	Current study	Melero et. al [10]	Fu et.al [70]	Feyzi et. al [71]
Oil/fat feedstock	UCO/Oleic acid	Crude palm oil	Rapeseed oil/Oleic acid	Sunflower oil
Methanol to oil ratio	15:1	20:1	10:1	12:1
Type of catalyst	$TiO_2/PrSO_3H$	SBA-15-$PrSO_3H$	β-Cyclodextrin-SO_3H	$CsH_3PW_{12}O_{40}$/Fe-SiO_2
Amount of catalyst%	4.5	6	5.0	3
Agitation speed, RPM	600	Not reported	500	500
Time, hrs	9	4	12	4
Temperature, °C	60	140	60-85	60
FAME yield %	98.3	95	90.82	81
BET surface area, $m^2.g^{-1}$	38.59	666	38.2	237.5
Mean pore size Å	245.46	82	---	173.4
Average particle size, nm	23.1	Not reported	1000	38-42
Catalyst recycled	4	2	6	Not reported